PERGAMON

International Journal of Heat and Mass Transfer 45 (2002) 1093–1107

International Journal of HEAT and MASS TRANSFER

www.elsevier.com/locate/ijhmt

# Heat (mass) transfer in rectangular cross-sectioned two-pass channels with an inclined divider wall

M. Hirota [a,*], H. Fujita [a], L. Cai [a], H. Nakayama [a], M. Yanagida [b], A. Syafa'at [a]

[a] *Department of Mechanical Engineering, Nagoya University, Chikusa-ku, Nagoya 464-8603, Japan*
[b] *Interior Design Department, ARACO Co. Ltd., Yoshihara-cho, Toyota 473-8512, Japan*

Received 26 January 2001; received in revised form 20 April 2001

**Abstract**

Heat transfer characteristics in rectangular cross-sectioned two-pass channels with an inclined divider (inner) wall have been examined experimentally. Local heat (mass) transfer rates were measured by the naphthalene sublimation method; seven kinds of divider inclination angles were tested for three turn clearances under the Reynolds numbers of $(2.0–5.0) \times 10^4$. The influence of the inclined divider wall on the local heat transfer characteristics is discussed in detail. Then, the optimum combination of the inclination angle and the turn clearance is examined based on the trade-off between the heat transfer enhancement and pressure loss penalty, and on the improvement of uniformity in the distribution of local heat transfer rates. 

## 1. Introduction

Rectangular cross-sectioned two-pass or three-pass channels connected by sharp 180° turns are often used as flow passages in heat exchanging equipment. One of their typical applications is in internal cooling passages of gas-turbine blades exposed to high-temperature gas flow [1–3]. The flow characteristics in such a serpentine channel with sharp turns are very complex because, in addition to the secondary flow that presents in the turning flow, the flow separation and reattachment occur in and after the turn section [4]. As a result, the local heat transfer rates around the turn change steeply over a short distance, and thus the degree of non-uniformity in their distribution is considerably large there [5–9]. The non-uniform distribution of the local heat transfer rates causes large temperature gradients and large thermal stresses over the heat transfer surface, and thus it affects the life of the equipment. Therefore, detailed data on the local heat transfer characteristics of the channels are indispensable for a critical design of heat exchanging equipment. Moreover, they are also helpful as the database for a better understanding of the heat transport process in complex turbulent flows. In response to such demand, many studies have been conducted to date on turbulent heat and mass transfer in rectangular cross-sectioned serpentine channels with sharp 180° turns [1–13]. The present authors also measured the distributions of the local heat (mass) transfer rates over all the walls of the channel by the naphthalene sublimation method, and made clear the influences of the turn clearance and flow-inlet condition on the heat transfer characteristics [14–16].

In these earlier studies, the divider (inner) wall of the channel has been settled parallel to the outer walls. In practical thermal equipment, however, it may be sometimes encountered that the divider wall is settled obliquely with respect to the outer walls as illustrated in Fig. 1. In this case, the primary flow in the convergent (or divergent) sections before and after the turn is accelerated (or decelerated) due to the streamwise change of the channel cross-sectional area. The influence of such acceleration or deceleration of the primary flow is then reflected on the secondary flow distribution, and on the flow separation and reattachment around the turn as well. As a result, the local heat transfer characteristics in the channel can be considerably changed from those in the standard parallel-wall channel.

* Corresponding author. Tel.: +81-52-789-2702; fax: +81-52-789-2703.
*E-mail address:* hirota@mech.nagoya-u.ac.jp (M. Hirota).

0017-9310/02/$ - see front matter 
PII: S0017-9310(01)00212-5

**Nomenclature**

| | |
|---|---|
| $C$ | turn clearance, see Fig. 3 [mm] |
| $C^*$ | dimensionless turn clearance $= C/W$ |
| $D$ | naphthalene–air molecular diffusion coefficient [$m^2/s$] |
| $d_h$ | hydraulic diameter of the channel at the channel entrance $= 2W/3$ ($= 33.3$ mm) |
| $h_m$ | local mass transfer coefficient [m/s] |
| $K$ | coefficient of pressure loss, defined by Eq. (2) |
| $K_S$ | coefficient of pressure loss for the standard channel ($\alpha = 0°$ and $C^* = 1.0$) |
| $K^+$ | coefficient of pressure loss normalized by $K_S$ |
| $Re$ | Reynolds number defined at the channel entrance $= U_b d_h/v$ |
| $Sh$ | local Sherwood number $= h_m d_h/D$ |
| $Sh_B$ | block-averaged Sherwood number, defined by Eq. (3) |
| $Sh_m$ | mean Sherwood number |
| $Sh_{mS}$ | mean Sherwood number for the standard channel ($\alpha = 0°$ and $C^* = 1.0$) |
| $Sh_m^+$ | mean Sherwood number normalized by $Sh_{mS}$ |
| $Sh_{m0}$ | mean Sherwood number for turbulent flow in a straight pipe, calculated by Eq. (1) |
| $U_b$ | bulk velocity of air at the channel entrance [m/s] |
| $W$ | spanwise length of the long-side wall at the channel entrance ($= 50$ mm) |

*Greek symbols*

| | |
|---|---|
| $\alpha$ | inclination angle of the divider wall, see Fig. 3 [degree] |
| $\Delta P$ | pressure difference between two pressure taps $PT_1$ and $PT_2$ [Pa] |
| $v$ | kinematic viscosity of air [$m^2/s$] |
| $\rho$ | density of air [$kg/m^3$] |
| $\sigma$ | standard deviation of $Sh$, calculated by Eq. (4) |

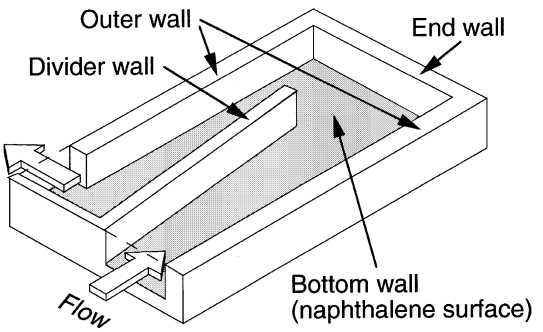


Fig. 1. Test section ($\alpha > 0°$).

In applying the serpentine channels to practical equipment used under severe thermal conditions, it is important not only to achieve higher heat transfer rates with lower pressure loss, but also to increase the uniformity in the distributions of the local heat transfer rates for decreasing the thermal stresses. Most of the earlier studies, however, have focused only on the trade-off between the heat transfer enhancement and the pressure loss penalty. Very little attention has been directed to the improvement of the uniformity in the distribution of local heat transfer rates. In the serpentine channels with an inclined divider wall, by inclining the divider wall appropriately, it may be possible that both the enhancement of heat transfer and the improvement of local heat transfer uniformity be achieved concurrently without a serious increase of pressure loss.

With these points as background, we have made an experimental study on forced convection heat transfer in the two-pass rectangular channels with an inclined divider wall. As the first step of the study, the local heat (mass) transfer rates on the long-side wall of the channel (see Fig. 1) have been measured by the naphthalene sublimation method to elucidate whether or not the inclined divider wall is effective to the enhancement of heat transfer and/or the improvement of the local heat transfer uniformity. Seven kinds of inclination angles have been tested for three turn clearances under the Reynolds number range of $(2.0–5.0) \times 10^4$. In this paper, the influence of the inclined divider wall on the heat transfer characteristics is discussed in detail based on the distribution maps of local Sherwood number. Then, the optimum combination of the inclination angle and the turn clearance is determined that can achieve both the enhancement of heat transfer and the improvement of heat transfer uniformity concurrently without a large pressure loss penalty.

## 2. Experiments

Fig. 2 shows a schematic diagram of the experimental apparatus. The flow loop is essentially the same as that

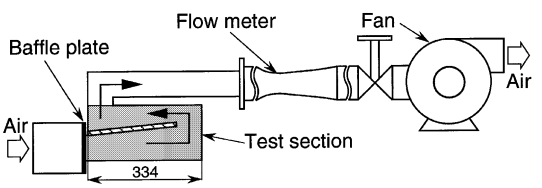


Fig. 2. Schematic diagram of the experimental apparatus.

used in the preceding studies [14–16]. Air flows into the test channel through a settling chamber. A baffle plate is placed at the entrance of the test channel; the air flow entering the test channel is separated at its sharp edge and thus has an abrupt contraction-entrance condition with strong turbulence [16,17]. The heat (mass) transfer rate is measured in the darkened region in the figure, which is located just downstream of the settling chamber, by the naphthalene sublimation method [18]. Air contaminated by naphthalene vapor is then exhausted from the building by a turbofan.

A schematic illustration of the test section is shown in Fig. 1. The test channel has a rectangular cross-section; the spanwise length of the short-side walls (divider, outer, and end walls) is 25 mm throughout the test section, while that of the long-side walls (top and bottom walls) is 50 mm at the channel entrance and it varies in the flow direction depending on the inclination angle of the divider (inner) wall. The channel aspect ratio at the entrance is 2:1 in all the channels tested here. This aspect ratio was chosen because in the earlier experiments we obtained detailed results of heat (mass) transfer in parallel-wall channels with an aspect ratio of 2:1 [14–16], which were useful as a database to examine the influence of the inclined divider wall in the present study. (Since the heat transfer characteristics in the channels can be influenced by the channel aspect ratio [9], the authors are now planning to conduct the measurements in the channels with different aspect ratios as a next step of this study.) The hydraulic diameter defined at the channel entrance, $d_h$, is 33.3 mm. The length from the channel entrance to the end wall is 334 mm $\approx 10d_h$. The surface of one long-side wall (bottom wall) was coated by naphthalene to measure the local mass transfer rates on it. The other long-side wall and all the short-side walls were made of smooth aluminum plates. From a preliminary experiment, it was confirmed that the *Sh* distribution obtained under this situation agreed well with that obtained in the channel which had the naphthalene-coated surfaces on the both long-side walls. We also confirmed in the standard channel ($\alpha = 0°$ and $C^* = 1.0$), the short-side walls of which were coated by naphthalene, that the mass transfer from the short-side walls did not exert appreciable influence on the distribution of mass transfer rates on the long-side wall. Thus, it is thought that the results of mass transfer obtained under the present experimental setup are applicable to the case in which all the channel walls are coated by naphthalene.

Fig. 3 shows the details of the mass transfer surface in the test section, i.e., the bottom wall in Fig. 1. The gray region corresponds to the naphthalene surface. The divider wall is made of a smooth aluminum plate of 10 mm thickness, and it is inclined with respect to the outer walls. The inclination angle of this divider wall, denoted as $\alpha$ in the figure, was changed from $-6°$ (clockwise direction in the figure) to $+6°$ (counter-clockwise direction) at 2° intervals; totally seven inclination angles including $\alpha = 0°$ (parallel to the outer walls) were tested in this study. We call the channel with $\alpha > 0°$ divergent channel, and that with $\alpha < 0°$ convergent channel. The channel with $\alpha = 0°$ is named as parallel-wall channel. In all the channels, the edge of the divider-wall tip is parallel to the end wall. The turn clearance denoted $C$ in Fig. 3 was changed as 30, 50, and 70 mm. It should be noted that, in the parallel-wall channel with $C = 50$ mm, the turn clearance is just equal to the spanwise length of the long-side wall. This channel has a standard geometry that has been adopted most often in earlier studies [4–16], and thus it is called standard channel. In this paper, the turn clearance is made dimensionless ($C^*$) by that of this standard channel; namely, $C^* = C/W = 0.6$, 1.0, and 1.4 for $C = 30$, 50, and 70 mm, respectively.

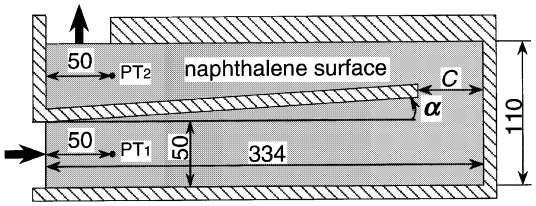


Fig. 3. Details of the naphthalene surface (bottom wall, $\alpha > 0°$) (pressure taps $PT_1$ and $PT_2$ are on an acrylic resin wall).

The measurement procedure of the local mass transfer coefficient $h_m$ is the same as that of the earlier experiments [14–16]. It was calculated from the difference in the naphthalene surface profiles before and after each data run, which were measured by a digital linear gage with a resolution of 1 μm. It was passed over the naphthalene surface by a computer-controlled two-dimensional positioning gear at 0.2 mm pitch in the streamwise direction and 2.5 mm pitch in the spanwise direction. We also measured the pressure distribution to calculate the pressure loss coefficient of the channel. It was measured under a non-sublimating condition by replacing the naphthalene-coated bottom wall with an acrylic resin wall, on which the pressure taps of 0.4 mm diameter were distributed on the spanwise centerline [15]. The locations of the pressure taps used to obtain the pressure difference $\Delta P$, which is included in the definition of the pressure loss coefficient $K$, are shown in Fig. 3 as $PT_1$ and $PT_2$. The maximum uncertainties in the evaluation of the local mass transfer coefficient and the pressure difference were estimated to be about ±6% and ±4%, respectively. The experiments were conducted under the Reynolds number range of $2.0 \times 10^4$–$5.0 \times 10^4$, where $Re$ was defined with $U_b$ and $d_h$ at the channel entrance. In this paper, the main results are shown for $Re = 3.5 \times 10^4$.

## 3. Results and discussion

### 3.1. Mean Sherwood number and coefficient of pressure loss

Fig. 4 shows the variation of the mean Sherwood number $Sh_m$ against the inclination angle of the divider wall $\alpha$ obtained for all turn clearances under a single $Re$ of $3.5 \times 10^4$. Here, the mean Sherwood number for fully developed turbulent flow in a straight pipe calculated by the following modified Dittus–Boelter's correlation [19] (denoted as $Sh_{m0}$) is about 150 for $Re = 3.5 \times 10^4$:

$$Sh_{m0} = 0.0243 Re^{0.8} Sc^{0.4} \quad (Sc : \text{Schmidt number}). \tag{1}$$

Thus, it follows that the sharp turn enhances the mean heat (mass) transfer rates up to 1.5–2 times that of the straight pipe.

In the convergent channels of $\alpha < 0°$, $Sh_m$ increases in proportion to $|\alpha|$, and $Sh_m$ for $\alpha = -6°$ is about 20–30% larger than that for the parallel-wall channels. On the other hand, in the divergent channels of $\alpha > 0°$, $Sh_m$ is nearly constant ($C^* = 1.0$ and 1.4) or decreased ($C^* = 0.6$) against $\alpha$. In general, $Sh_m$ shows higher values as the turn clearance is decreased. The dependency of $Sh_m$ on $C^*$ is, however, rather weak in the divergent channels, and $Sh_m$ for $\alpha = +6°$ is almost independent of $C^*$.

The coefficient of pressure loss of the channel $K$ [1], which is defined by Eq. (2), was calculated from the pressure distribution, and the result for $Re = 3.5 \times 10^4$ is shown in Fig. 5.

$$K = \frac{2\Delta P}{\rho U^2}. \tag{2}$$

$\Delta P$ is the pressure difference between two pressure taps $PT_1$ and $PT_2$; the former is located 50 mm downstream from the channel entrance, and the latter is 50 mm upstream from the end of the test section (see Fig. 3). In

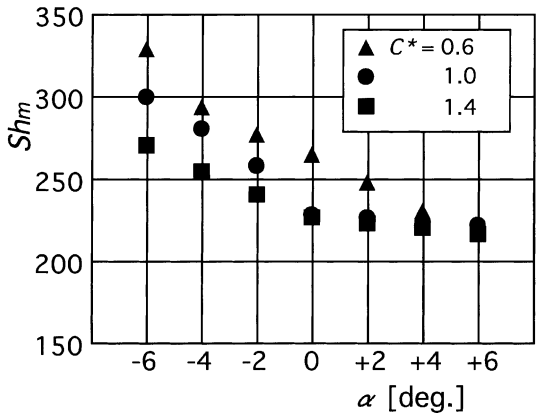


Fig. 4. Mean Sherwood number ($Re = 3.5 \times 10^4$).

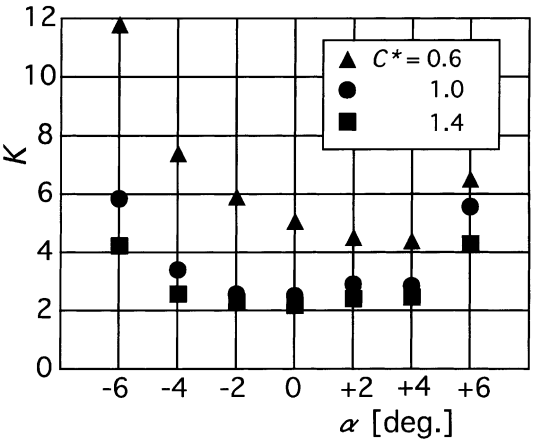


Fig. 5. Coefficient of pressure loss ($Re = 3.5 \times 10^4$).

both the convergent and the divergent channels, $K$ increases as $|\alpha|$ is increased or as $C^*$ is decreased. Similar to the case of the parallel-wall channel [15], the values of $K$ for $C^* = 0.6$ are considerably larger than those for a wider turn clearance. This is attributed to the large pressure loss that arises when the flow passes through a narrower turn clearance. Moreover, the dependence of $K$ on $\alpha$ in the channel with $C^* = 0.6$ is somewhat different from that in other channels; $K$ becomes minimum not in the case of $\alpha = 0°$ but in $\alpha = +4°$. The mechanism for such unique behavior of $K$ in the channel with $C^* = 0.6$ is not clear at the present stage. From the pressure distributions measured on the wall, however, it could be estimated that the scale of the separation bubble after the turn exit became smallest at $\alpha = +4°$ in the channel with $C^* = 0.6$; this may be a reason for the minimum $K$ at $\alpha = +4°$ for $C^* = 0.6$. As a whole, the difference in $K$ values ascribed to $C^*$ is smaller in the divergent channels than in the convergent channels; this tendency is quite similar to that of the $Sh_m$ distribution described above.

A comparison of $Sh_m$ and $K$ leads to a conclusion that, from the viewpoint of a trade-off between the heat transfer enhancement and the pressure loss penalty, the convergent channel is better than the divergent channel for the case of $C^* = 1.0$ and 1.4. The heat transfer performance of the channel with $C^* = 0.6$ seems to be inferior to that of the other channels with larger $C^*$. Details on the optimum inclination angle and turn clearance are discussed later in this paper.

### 3.2. Block-averaged Sherwood number

In order to grasp the global characteristics of the local heat transfer, we have divided the mass transfer surface into 14 blocks as shown in Fig. 6 and calculated the values of Sherwood number averaged in each block

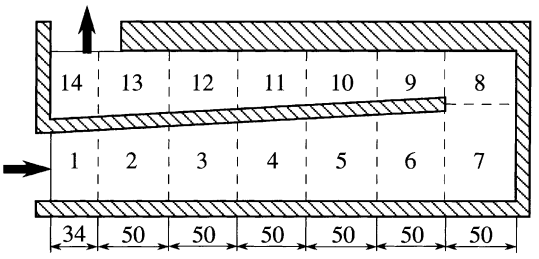


Fig. 6. Definition of blocks ($C^* = 1.0$ and $\alpha > 0°$).

[12]. This semi-regional Sherwood number, denoted as block-averaged Sherwood number $Sh_B$, is defined by the following equation:

$$Sh_B = \frac{1}{\Delta S}\int\int_{\Delta S} Sh\,dS. \tag{3}$$

$\Delta S$ denotes the surface area of each block, and it varies depending on $\alpha$ as recognized from Fig. 6. The boundary between Block 7 and Block 8 also moves depending on $\alpha$. Here it should be noted that this definition of $Sh_B$ is not so usual in the case of heat transfer experiments such as stainless-foil heating, in which the block-averaged Nusselt number is obtained from the difference of the bulk temperatures of air flow before and after the block. The definition of Eq. (3) was used here because the direct measurement of the averaged-concentration difference before and after the block was impossible in the present experimental setup with the naphthalene sublimation method. In this method, the wall boundary condition corresponds to the constant-wall-temperature heating in heat transfer experiments, and thus the values of $Sh_B$ calculated by Eq. (3) agree with those obtained from the bulk-temperature (averaged-concentration) difference.

The streamwise variations of $Sh_B$ obtained for $C^* = 1.0$ and $Re = 3.5 \times 10^4$ are shown in Figs. 7 and 8 for the divergent and the convergent channels, respectively. The abscissa shows the block number defined in

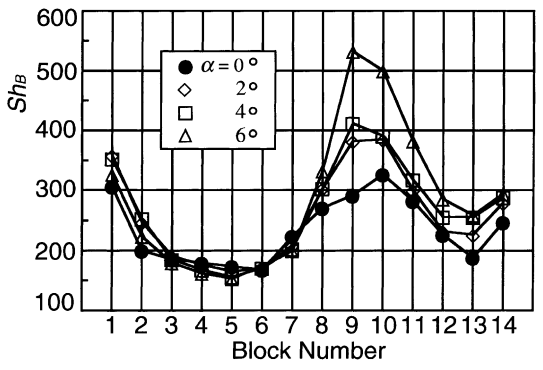


Fig. 7. Block-averaged Sherwood number in the divergent channels ($C^* = 1.0$, $Re = 3.5 \times 10^4$).

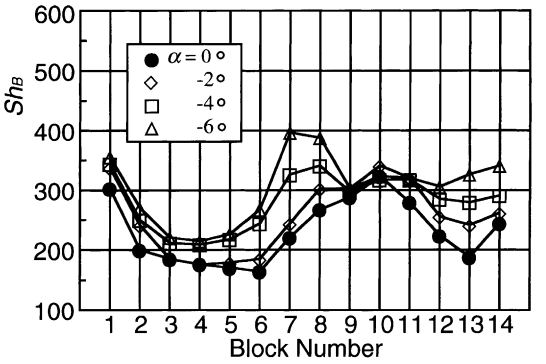


Fig. 8. Block-averaged Sherwood number in the convergent channels ($C^* = 1.0$, $Re = 3.5 \times 10^4$).

Fig. 6. It was confirmed that $Sh_B$ for $C^* = 0.6$ and 1.4 showed qualitatively similar distributions to these figures.

In the divergent channels, the distributions of $Sh_B$ in Blocks 1–7 are similar to that in the parallel-wall channel, and the characteristics of $Sh_B$ distribution for smaller $\alpha$ agree well with those for larger $\alpha$. It thus follows that the influence of $\alpha$ on $Sh_B$ values does not appear so clearly in the upstream half of the test section despite the decrease of the primary flow velocity caused by the divergence of the channel. $Sh_B$ shows the local maximum at the entrance of the channel, and it decreases in the streamwise direction up to Block 5. Then $Sh_B$ begins to increase in the turn section (Blocks 7 and 8), and reaches the maximum in Block 9 ($\alpha = +4°$ and $+6°$) located just downstream of the turn exit or in Block 10 ($\alpha = 0°$ and $+2°$) a few $d_h$ downstream from the turn exit. $Sh_B$ after Block 10 decreases in the streamwise direction, and it increases again in Block 14 due to the influence of the second turn connected at the exit of the test section. In the downstream half of the test section (Blocks 8–14), contrary to the upstream half, the values of $Sh_B$ increase as $\alpha$ is increased; this increase of $Sh_B$ is most pronounced in Blocks 9 and 10, in which $Sh_B$ attains the maximum.

In the convergent channels shown in Fig. 8, the influence of $\alpha$ on $Sh_B$ can be observed clearly in the whole region except for Blocks 9 and 10, and thus the qualitative characteristics of $Sh_B$ distribution, as well as quantitative ones, are quite different from those in the divergent channels. In Blocks 1–4, $Sh_B$ decreases in the downstream direction; it shows larger values as $|\alpha|$ is increased because of higher degree of the acceleration in the primary flow. $Sh_B$ begins to increase at Block 5, and attains the first local maximum in Block 7 ($\alpha = -6°$) or Block 8 ($\alpha = -2°$ and $-4°$) in the turn section. Then $Sh_B$ once again decreases in Block 9, and increases again in Block 10 to attain the second local maximum. The first local maximum becomes larger with the increase of $|\alpha|$,

whereas the second one is almost constant irrespective of $\alpha$. It is also observed that, in the channels with $\alpha = -4°$ and $-6°$, the first local maximum is larger than the second one. After Block 11, $Sh_B$ decreases in the streamwise direction; similar to the case of Blocks 1–4, $Sh_B$ shows higher values in the channel with larger $|\alpha|$. A close comparison of $Sh_B$ values in this region of Figs. 7 and 8 reveals that higher values of $Sh_B$ are maintained after Block 11 in the convergent channels than in the divergent channels.

From these $Sh_B$ distributions, it is thought that in the divergent channels the degree of non-uniformity in the distribution of local heat transfer rates is intensified, because the maximum $Sh_B$ in Block 9 or 10 further increases by inclining the divider wall to the positive direction. On the contrary, in the convergent channels, $Sh_B$ increases in the whole region except for Blocks 9 and 10, and thus such non-uniformity of the local heat transfer rates may be lessened. The uniformity in the distribution of local heat transfer rates is discussed quantitatively in detail later.

### 3.3. Local Sherwood number distributions for a medium turn clearance ($C^* = 1.0$)

The distributions of local Sherwood number $Sh$ obtained in the channels with different inclination angles are presented in the form of a two-dimensional map. In all the maps of Figs. 9–11, the turn clearance is at a medium value of $C^* = 1.0$ and $Re$ is $3.5 \times 10^4$. At first $Sh$ distribution in the parallel-wall channel is reviewed briefly [15], then $Sh$ maps obtained in the divergent and the convergent channels are presented. Note that all the maps presented here show the $Sh$ values normalized by the mean Sherwood number for the fully developed turbulent flow in a straight pipe, $Sh_{m0}$, given by Eq. (1).

#### 3.3.1. Parallel-wall channel

Fig. 9 shows a distribution of $Sh/Sh_{m0}$ obtained in the parallel-wall channel [15]. The variations in the values of $Sh/Sh_{m0}$ are shown as contrasting light and dark areas. The map becomes whiter as $Sh/Sh_{m0}$ is increased; the very high mass-transfer region of $Sh/Sh_{m0} > 3.0$ is shown in white. The arrows present the flow direction at the entrance and exit of the test section. The broken lines show the boundaries of the blocks defined in Fig. 6.

In the straight section before the turn (Blocks 1–6), $Sh$ shows the local maximum at the entrance, then it decreases in the flow direction due to the development of the concentration boundary layer. In the turn section (Blocks 7 and 8), $Sh$ increases gradually in the flow direction; near the end wall in Block 7 and near the outer wall in Block 8, it rises very steeply to attain the local maximums. These local maximums of $Sh$ are caused by the following mechanism [15]. In Block 7, the flow that enters the turn section first impinges on the end wall. The direction of this flow is then changed by this wall, and the flow partly impinges again on the bottom wall. This second flow impingement causes the local maximum of $Sh$ near the end wall in Block 7. The high-$Sh$ region near the outer wall in Block 8 is also caused by a similar mechanism.

In the straight section after the turn (Blocks 9–14), a region of relatively low $Sh$ appears near the divider-wall tip in Block 9. $Sh$ then increases in the streamwise direction, and attains the local maximum in Block 10. This $Sh$ distribution suggests that the flow is separated at the divider-wall tip, forms a separation bubble with low heat (mass) transfer rates along the divider wall in Block 9, and then reattaches in Block 10. From a preceding measurement of $Sh$ on the short-side walls, it was found that the flow separated at the divider-wall tip reattaches again on the divider wall in Block 10 [15]. After Block 11, $Sh$ is decreased in the streamwise direction; if com-

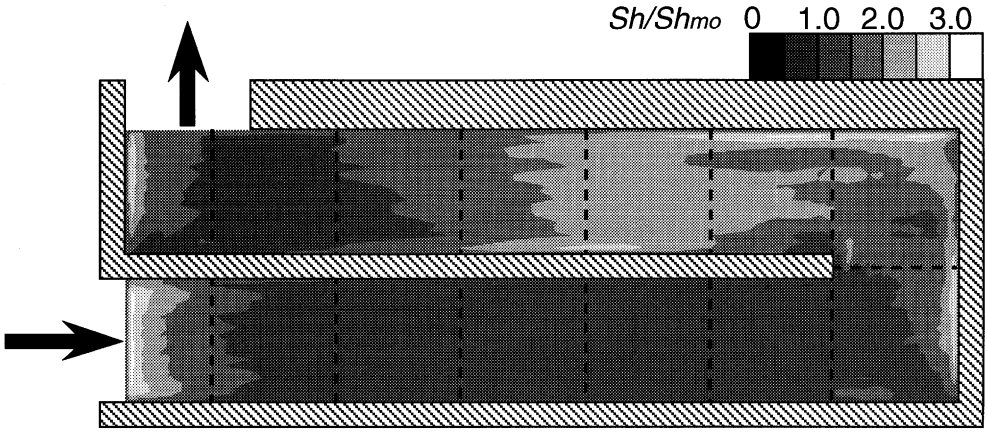


Fig. 9. Distribution of $Sh/Sh_{m0}$ in the parallel-wall channel with $C^* = 1.0$ ($Re = 3.5 \times 10^4$).

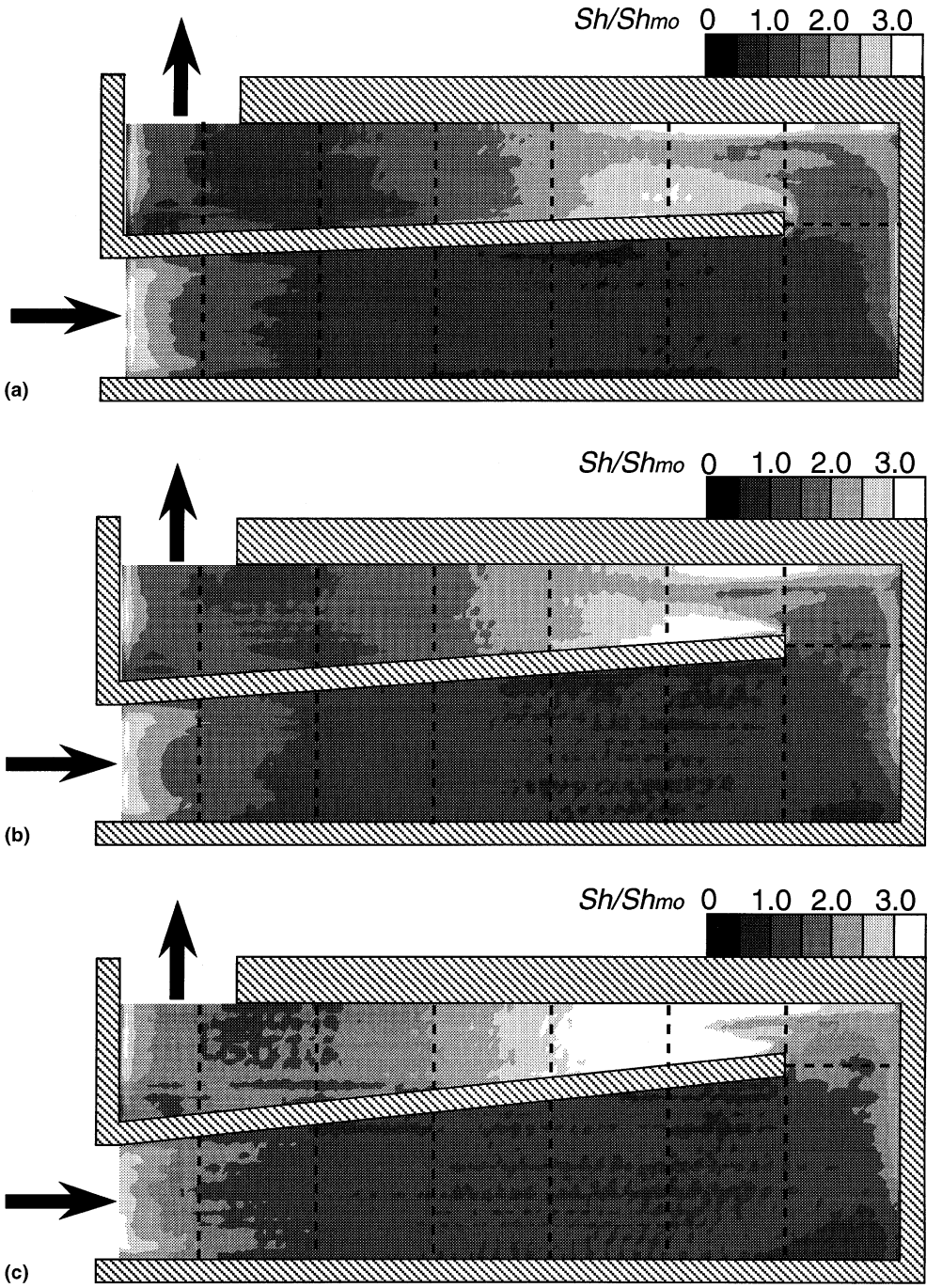


Fig. 10. Distributions of $Sh/Sh_{m0}$ in the divergent channels with $C^* = 1.0$ ($Re = 3.5 \times 10^4$): (a) $\alpha = +2°$; (b) $\alpha = +4°$; (c) $\alpha = +6°$.

pared at the same streamwise location, $Sh$ in the outer-wall side shows larger values than that in the divider-wall side. This suggests that the primary flow velocity near the outer wall in this region is higher than that near the divider wall.

*3.3.2. Divergent channel* ($\alpha > 0°$)

Figs. 10(a), (b), and (c) show the maps of $Sh/Sh_{m0}$ obtained in the divergent channels with $\alpha = +2°$, +4°, and +6°, respectively. In the divergent section before the turn of all the channels, there appear spots of

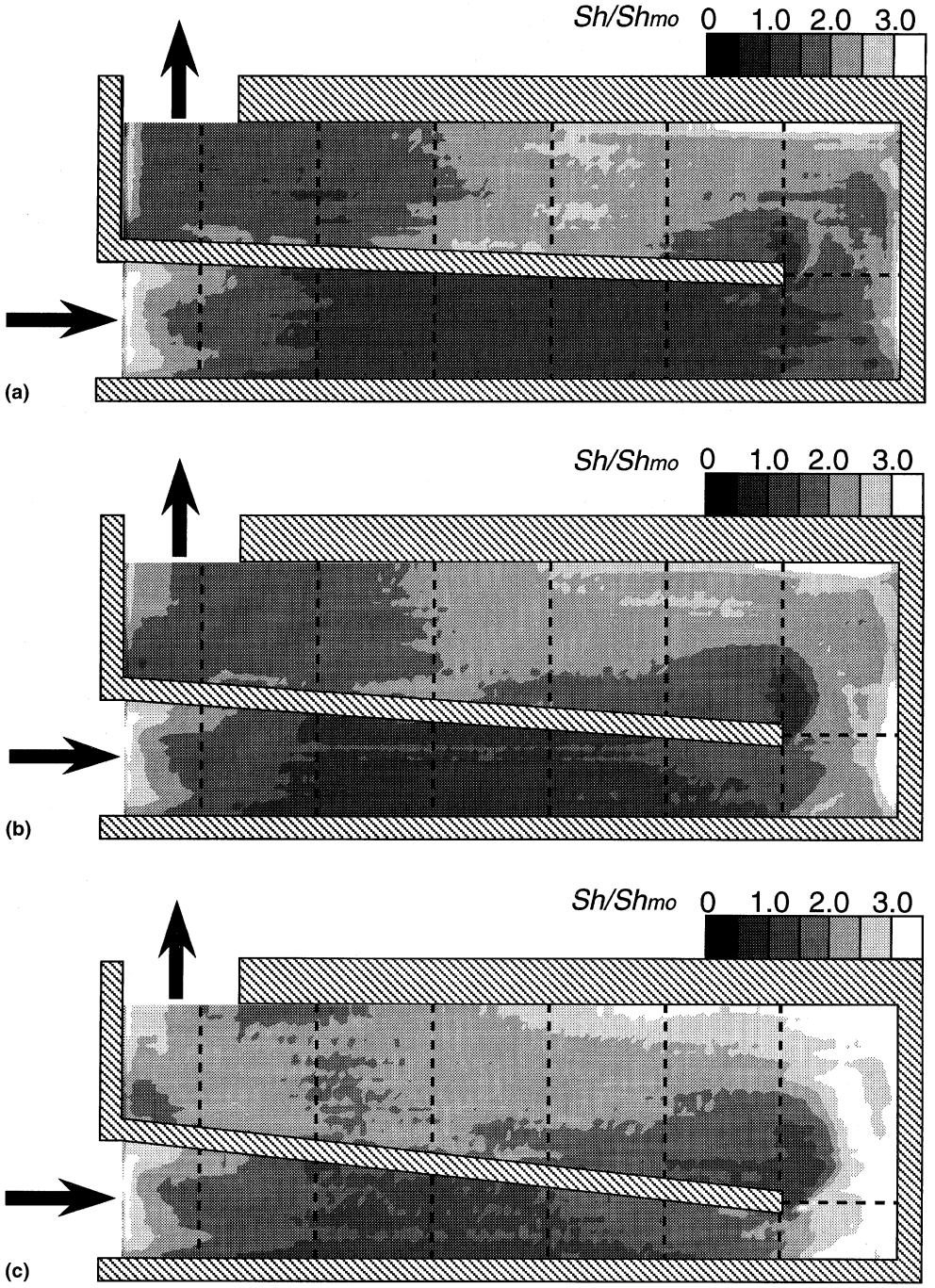


Fig. 11. Distributions of $Sh/Sh_{m0}$ in the convergent channels with $C^* = 1.0$ ($Re = 3.5 \times 10^4$): (a) $\alpha = -2°$; (b) $\alpha = -4\sigma$; (c) $\alpha = -6°$.

relatively low $Sh$ in Blocks 4 and 5; these low-$Sh$ spots tend to increase in area as $\alpha$ is increased. Such deterioration of heat (mass) transfer in this section is ascribed to the deceleration of the primary flow.

In the upstream half of the turn section (Block 7), a low-$Sh$ region can be observed near the first outer corner and it occupies larger area as $\alpha$ is increased. This is because a separation bubble is formed in this corner region, and the flow tends to be stagnant there. In the

downstream half of the turn section, on the other hand, *Sh* becomes larger as $\alpha$ is increased and shows higher values than in Block 7.

The characteristics of *Sh* distribution after the turn are much influenced by $\alpha$. At first, the *Sh* distribution for $\alpha = +2°$ shown in Fig. 10(a) is examined in detail. Near the divider-wall tip, a region of relatively low *Sh* value corresponding to the separation bubble is observed, but its scale is considerably smaller than that in the parallel-wall channel. In Block 9, *Sh* shows remarkably large values outside this separation bubble ($Sh/Sh_{m0} > 2.5$) and near the outer wall ($Sh/Sh_{m0} > 3.0$); the high-*Sh* region in the divider-wall side (outside the separation bubble) occupies a major part of Block 10 as well. Such increase of *Sh* in Blocks 9 and 10 is caused by the acceleration of the primary flow which passes through a narrower turn exit, and by high turbulence which is produced in the shear layer outside the separation bubble. After Block 11, *Sh* is decreased as the flow proceeds downstream. The values of *Sh* in this region of this divergent channel are in the same level as those in the corresponding region of the parallel-wall channel.

As $\alpha$ is increased, as shown in Figs. 10(b) and (c) for $\alpha = +4°$ and +6°, respectively, the values of *Sh* after the turn become larger because the flow velocity at the turn exit is increased. In particular, the separation bubble near the divider-wall tip disappears and, in the channel of $\alpha = +6°$, the region of very high *Sh* ($Sh/Sh_{m0} > 3.0$) occupies almost the whole area of Blocks 9 and 10. As recognized from the $Sh_B$ distribution shown in Fig. 7 as well, the maximum *Sh* in the divergent channels of $\alpha = +4°$ and +6° appears in Block 9 located just downstream of the turn exit. After these high *Sh* values, *Sh* decreases rapidly in the flow direction. A comparison of Figs. 10(a), (b), and (c) reveals that *Sh* after Block 11 becomes larger as $\alpha$ is increased.

### 3.3.3. Convergent channel ($\alpha < 0°$)

The maps of $Sh/Sh_{m0}$ obtained in the convergent channels with $\alpha = -2°$, −4°, and −6° are shown in Figs. 11(a), (b), and (c), respectively. In the convergent section before the turn, the primary flow is accelerated due to the decrease of the cross-sectional area of the flow passage. Thus, *Sh* in this section becomes larger with the increase of $|\alpha|$, and it shows higher values than those observed in the corresponding region of the parallel-wall and the divergent channels.

In the turn section also, *Sh* in the convergent channels is generally larger than that in the other channels. Similar to the case of the parallel-wall channel, *Sh* shows the local maximums near the end wall in Block 7 and near the outer wall in Block 8. These high-*Sh* regions extend from the vicinity of the short-side walls into the inside of the turn section as $|\alpha|$ is increased; in the channel of $\alpha = -6°$, the region of $Sh/Sh_{m0} > 3.0$ occupies a rather large part of the turn section. It is thought that these high heat (mass) transfer rates near the short-side walls are caused by the same mechanism as that in the parallel-wall channel described above. As $|\alpha|$ is increased, the flow that impinges on the end wall (and on the bottom wall as well) has higher velocity and consequently the high-*Sh* regions extend inside the turn.

In Block 9 just after the turn, the low-*Sh* region corresponding to the separation bubble is observed near the divider wall. This low-*Sh* region occupies larger area than that appearing in the parallel-wall channel, and it extends upstream into the turn in case of large $|\alpha|$. On the other hand, in the outer-wall side of Blocks 9 and 10, *Sh* shows rather large values and it becomes larger with the increase of $|\alpha|$. These characteristics of *Sh* distribution in Fig. 11 suggest that, after the turn section of the convergent channel, a separation bubble with a large scale is formed along the divider wall, and the flow in the outer-wall side is accelerated due to the decrease of the substantial cross-sectional area of the flow passage. This accelerated flow enhances the heat (mass) transfer near the outer wall in these blocks.

As shown in Fig. 8, the values of $Sh_B$ in Blocks 9 and 10 of the convergent channels are nearly constant against $\alpha$. This is explained as follows based on Fig. 11. In Blocks 9 and 10, the low *Sh* region and the high *Sh* region coexist near the divider wall and the outer wall, respectively, and both of them become larger in scale as $|\alpha|$ is increased. In calculating $Sh_B$ based on Eq. (3), the influence of the low-*Sh* region is cancelled by its counterpart, and thus $Sh_B$ in these blocks shows nearly constant values irrespective of $\alpha$.

After Block 11, *Sh* shows higher values in the channel with larger $|\alpha|$. It should be also noted that *Sh* in this region of the convergent channels is generally larger than that in the corresponding region of the parallel-wall and the divergent channels.

## 3.4. Influence of the turn clearance on Sh distribution

The *Sh* distributions obtained in the channels with different $C^*$ are compared to one another. At first, the distributions of $Sh/Sh_{m0}$ in the divergent channels with $\alpha = +4°$ are shown in Figs. 12(a) and (b) for $C^* = 0.6$ and 1.4, respectively. As a whole, the global characteristics of *Sh* distributions in the divergent channels with different $C^*$ agree qualitatively with one another, albeit quantitative differences are observed in and after the turn as follows.

In the turn section for $C^* = 0.6$, the low-*Sh* region that is observed in the first outer corner for $C^* = 1.0$ and $C^* = 1.4$ is decreased in scale (this region cannot be expressed so clearly in Fig. 12(a) because of the limitation of the gradation resolution in the figure), and *Sh* shows higher values than that for larger $C^*$. In Blocks 9 and 10 after the turn also, *Sh* for $C^* = 0.6$ is remarkably larger than that for $C^* = 1.0$ and 1.4; this high *Sh* after

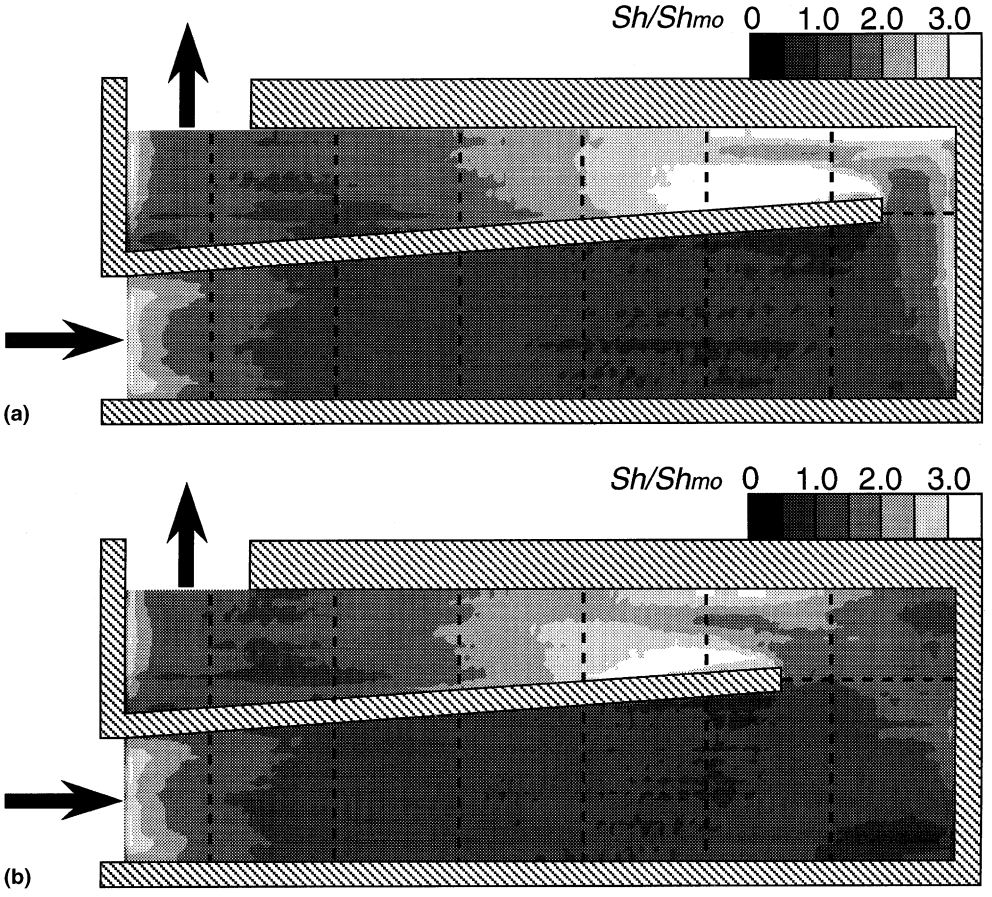


Fig. 12. Distributions of $Sh/Sh_{m0}$ in the divergent channels with $\alpha = +4°$ ($Re = 3.5 \times 10^4$): (a) $C^* = 0.6$; (b) $C^* = 1.4$.

the turn is brought about by the acceleration of the flow that passes through the narrow turn clearance and the narrow turn exit. After Block 11, however, such difference in *Sh* values attributed to the turn clearance is diminished, and *Sh* near the channel exit in Figs. 12(a) and (b) is almost in the same values as that for $C^* = 1.0$ (Fig. 10(b)). From a close comparison of *Sh* distributions in Blocks 11–14 in Fig. 10 and those in Fig. 12, it is found that the difference of *Sh* values caused by different $\alpha$ is larger than that caused by different $C^*$. Thus, it follows that the local heat (mass) transfer rates after Block 11 of the divergent channels are more influenced by $\alpha$ than by $C^*$.

Next, *Sh* maps of the convergent channels ($\alpha = -4°$) with $C^* = 0.6$ and 1.4 are shown in Fig. 13. For any $C^*$, a low-*Sh* region corresponding to the large separation bubble is formed near the divider-wall tip, whereas there appears a high-*Sh* region in the opposite outer-wall side. Thus, the *Sh* distributions for different $C^*$ are qualitatively similar to one another.

From a quantitative viewpoint, however, *Sh* values are much influenced by $C^*$. In the channel with $C^* = 0.6$, *Sh* in the downstream half of the channel is much larger than that for $C^* = 1.0$ and 1.4 because of the contraction and acceleration of the primary flow at the narrow turn clearance. In particular, *Sh* shows remarkably high values of $Sh/Sh_{m0} > 3.0$ in large areas near the outer wall in Blocks 7–10. On the other hand, in the channel with $C^* = 1.4$, the high-*Sh* regions in these blocks are considerably reduced in scale. Such dependence of *Sh* values on $C^*$ appears clearly in the region after Block 11 as well as in and just after the turn section. This tendency is quite different from that of the divergent channel mentioned above. It thus follows that, in the convergent channel, the influence of the turn clearance on *Sh* values after the turn appears more remarkably than in the divergent channel, and both $\alpha$ and $C^*$ are dominant to the local heat (mass) transfer characteristics after the turn.

### 3.5. Influence of Reynolds number on Sh distribution

The maps of $Sh/Sh_{m0}$ in the divergent channel ($\alpha = +4°$ and $C^* = 0.6$) obtained under $Re = 2.0 \times 10^4$ and $5.0 \times 10^4$ are shown in Figs. 14(a) and (b), respec-

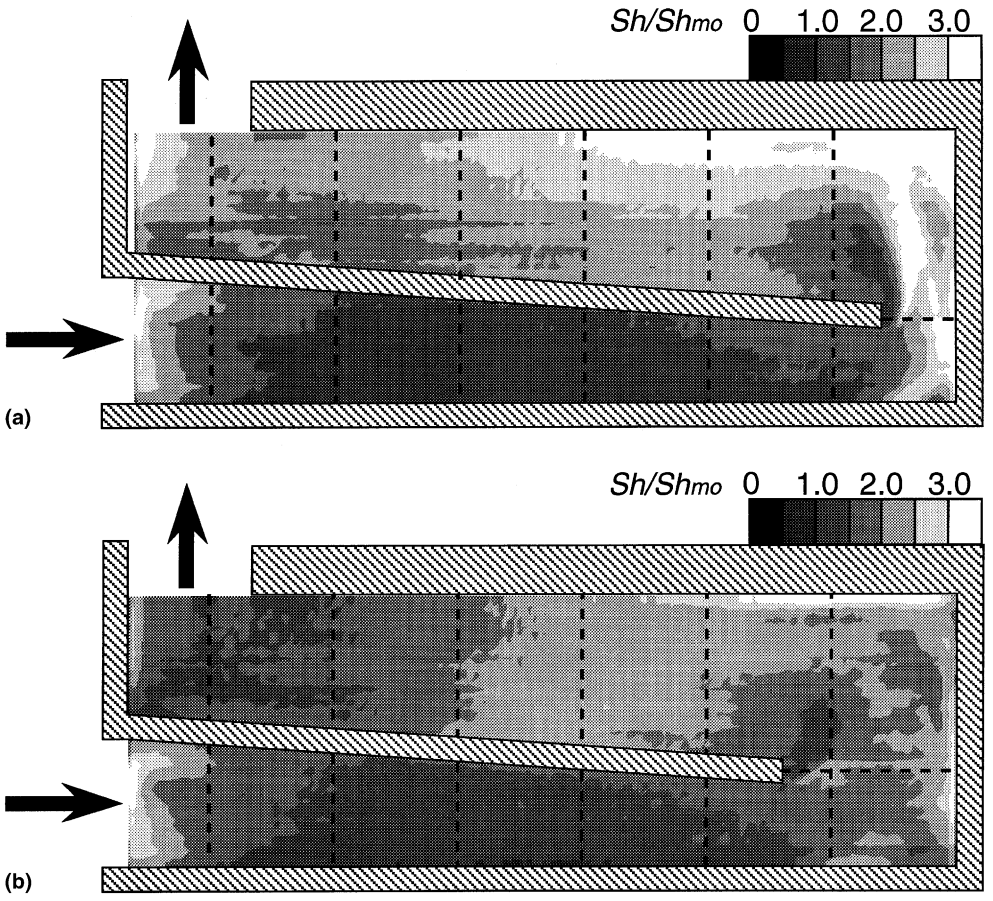


Fig. 13. Distributions of $Sh/Sh_{m0}$ in the convergent channels with $\alpha = -4°$ ($Re = 3.5 \times 10^4$): (a) $C^* = 0.6$; (b) $C^* = 1.4$.

tively. Fig. 15 shows the results of the convergent channel. As a whole, in both channels, the distributions of $Sh/Sh_{m0}$ obtained under different Reynolds numbers are similar to one another, qualitatively and quantitatively. That is, in the divergent channel, $Sh$ shows very large values of $Sh/Sh_{m0} > 3.0$ just after the turn section and the separation bubble is diminished. In the convergent channel, a large separation bubble accompanied by low $Sh$ is formed along the divider wall after the turn, and a high-$Sh$ region appears in the opposite outer-wall side. Similar results were obtained for other combinations of $C^*$ and $\alpha$. These results suggest that the data obtained under a single $Re$ condition can be reasonably applied to the estimation of the $Sh$ distribution for different Reynolds numbers.

## 4. Assessments of heat-transfer performance

When these channels are applied to practical equipment used under severe thermal conditions such as internal cooling passages of gas turbine blades, it is important not only to achieve higher mean heat transfer rates with lower pressure loss, but also to increase the uniformity in the distributions of the local heat transfer rates for decrease in the thermal stresses. Hence, in this study, we have evaluated the overall heat-transfer performance of the channels from the following two viewpoints: (1) trade-off between the heat transfer enhancement and the pressure loss penalty, and (2) degree of uniformity in the distribution of the local heat transfer rates. Then, the optimum condition of $\alpha$ and $C^*$ is determined that can achieve both the enhancement of mean heat transfer and the improvement of the local heat transfer uniformity concurrently without a considerable increase of pressure loss. Here, note that all the heat-transfer performance has been evaluated based on the data for $Re = 3.5 \times 10^4$.

At first, the trade-off between the heat transfer enhancement and the pressure loss penalty is examined based on $Sh_m$ and $K$ for $Re = 3.5 \times 10^4$. This kind of evaluation is usually made under a constraint of constant pumping power. In the present study, however, the experimental range of $Re$ was so limited that we could

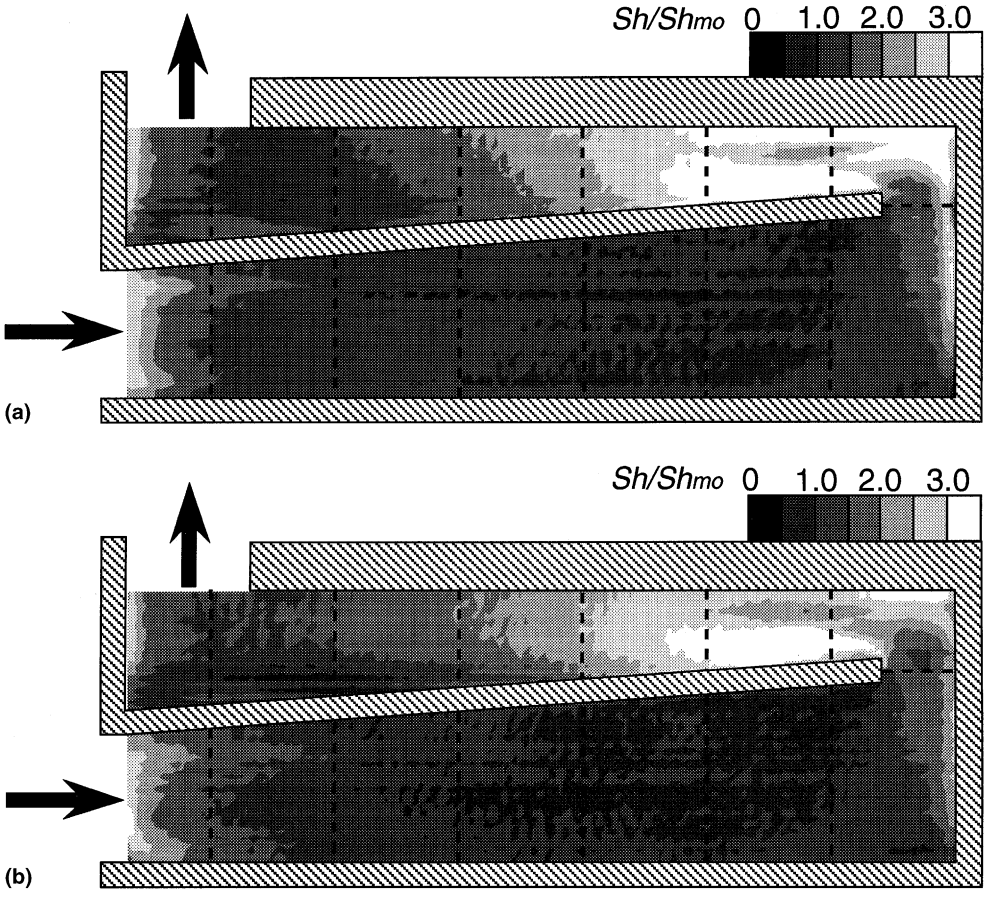


Fig. 14. Distributions of $Sh/Sh_{m0}$ in the divergent channels with $\alpha = +4°$ and $C^* = 0.6$: (a) $Re = 2.0 \times 10^4$; (b) $Re = 5.0 \times 10^4$.

not evaluate the heat-transfer performance of the channel under this constraint. Hence, as an alternative method, we made the evaluation based on $Sh_m^+/K^+$, where $Sh_m^+$ and $K^+$ denote the mean Sherwood number and coefficient of pressure loss normalized by $Sh_m$ and $K$ for the standard channel with $\alpha = 0°$ and $C^* = 1.0$, respectively (i.e., $Sh_m^+ = Sh_m/Sh_{mS}$ and $K^+ = K/K_S$). $Sh_m^+/K^+$ is equal to unity in the standard channel, and it becomes larger when a higher mean heat (mass) transfer rate and/or a lower pressure loss can be achieved. This parameter can be regarded as a measure to evaluate the trade-off between the heat transfer enhancement and the pressure loss penalty under a constraint of constant Reynolds number, i. e., a constraint of constant flow rate in the present experiment. Thus, the optimum condition of $\alpha$ and $C^*$ determined by this assessment can be somewhat different from that determined under a constraint of constant pumping power. Fig. 16 shows the variation of $Sh_m^+/K^+$ against $\alpha$ and $C^*$. In general, the value of $Sh_m^+/K^+$ is increased as the turn clearance is widened, and it reaches the maximum under the condition of $C^* = 1.4$ and $\alpha = 0°$ or $-2°$. Therefore, from a viewpoint of the trade-off between the heat transfer enhancement and the pressure loss penalty, the optimum channel specification is given by $C^* = 1.4$ and $\alpha = 0°$ or $-2°$.

Next, the uniformity in the distributions of local heat (mass) transfer rates is examined quantitatively. Although the qualitative trend of the uniformity in $Sh$ distributions can be understood from the distributions of $Sh_B$ and $Sh$ itself, we have evaluated it quantitatively based on the standard deviation of $Sh$ (denoted as $\sigma$) defined by the following equation:

$$\sigma = \sqrt{\frac{1}{N}\sum_{i=1}^{N}(Sh_i - Sh_m)^2}. \tag{4}$$

$N$ denotes the total number of the measuring points of $Sh$ in a channel, and it is about $6.5 \times 10^4$. It follows that lower values of $\sigma$ correspond to higher degree of uniformity in the distribution of local heat (mass) transfer rates. The variations of $\sigma/Sh_m$ against $C^*$ and $\alpha$ are shown in Fig. 17. As a general trend, $\sigma/Sh_m$ in the

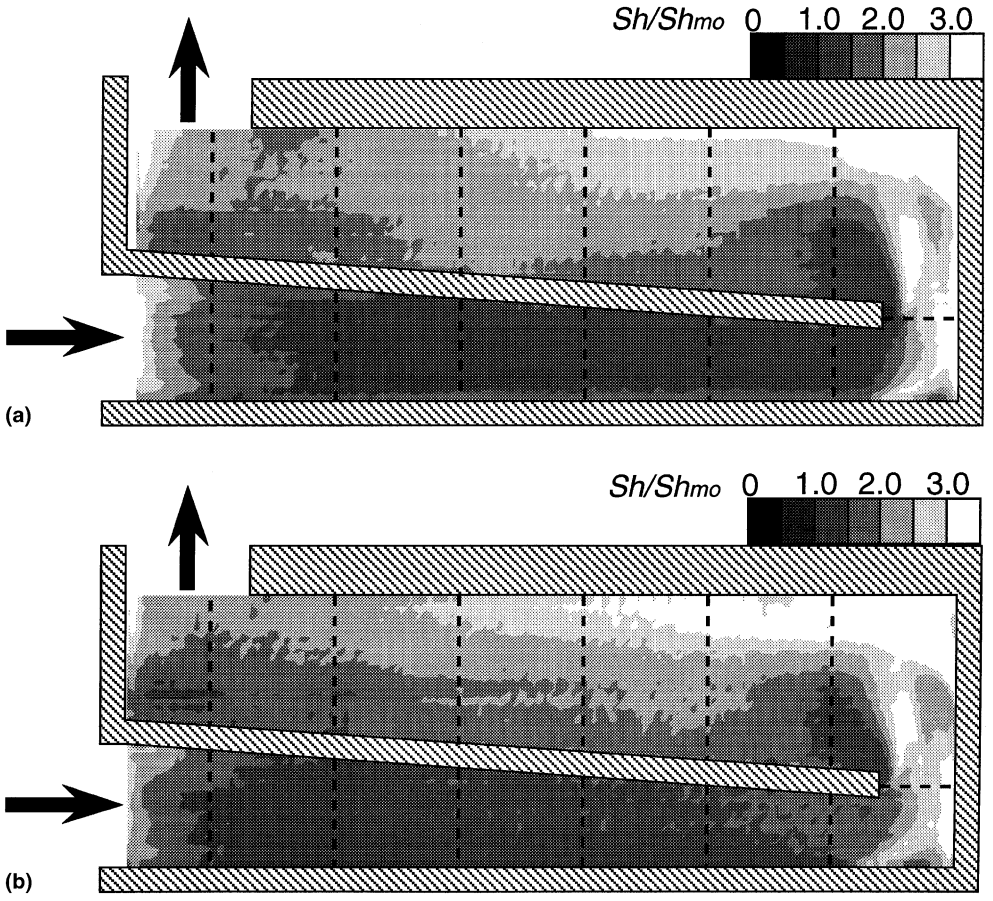


Fig. 15. Distributions of $Sh/Sh_{m0}$ in the convergent channels with $\alpha = -4°$ and $C^* = 0.6$: (a) $Re = 2.0 \times 10^4$; (b) $Re = 5.0 \times 10^4$.

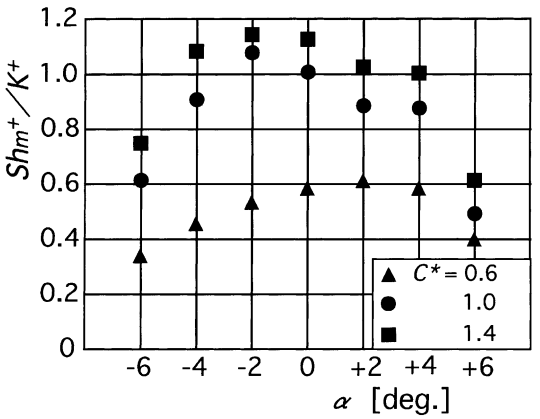


Fig. 16. Trade-off between the heat transfer enhancement and the pressure loss penalty.

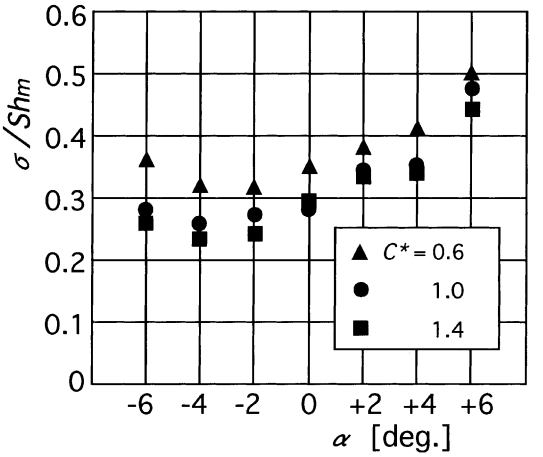


Fig. 17. Standard deviation of local Sherwood number.

convergent channels is smaller than that in the divergent channels, and it becomes lower as $C^*$ is increased. $\sigma/Sh_m$ can be minimized under the condition of $C^* = 1.4$ and $\alpha = -2°$ or $-4°$; this channel specification, i.e., convergent channels with a wide turn clearance, is thus the optimum one determined from the uniformity in the $Sh$

distribution. The tendency that $\sigma/Sh_m$ in the convergent channels generally shows smaller values than that in the divergent channels is consistent with the aforementioned observation of $Sh_B$.

The optimum values of $C^*$ and $\alpha$ determined based on $Sh_m^+/K^+$ overlap those determined from $\sigma/Sh_m$, and the overall heat-transfer performance of the channel becomes highest under the overlapped condition of $C^*$ and $\alpha$. Therefore it follows that, under the present experimental condition, the highest heat-transfer performance can be obtained in the channel with $C^* = 1.4$ and $\alpha = -2°$. With this channel specification, both the enhancement of mean heat transfer and the improvement of local heat transfer uniformity can be realized concurrently without a serious pressure loss penalty.

Here, it should be noted that the present results are obtained based on the *Sh* distribution on the long-side wall of the channel only; the optimum condition of $C^*$ and $\alpha$ may be slightly modified if the heat-transfer performance is evaluated based on *Sh* distributions on all the channel walls. Moreover, the heat transfer characteristics are significantly influenced by channel geometry such as aspect ratio, channel-entrance configuration, divider-wall thickness, corner radius, duct length, etc. Thus, the results obtained in the present study are not general to all types of two-pass channels but applicable only to the limited channel geometry described in Section 2. At the present stage, however, it would be possible to remark that, in applying the two-pass serpentine channels with a sharp turn to thermal equipment, the convergent channel with a wide turn clearance can be more advantageous than the divergent channel with a narrow turn clearance.

## 5. Conclusions

Heat (mass) transfer characteristics have been elucidated experimentally for turbulent flow in rectangular cross-sectioned serpentine channels with an inclined divider wall. The main results are summarized as follows.

1. The mean Sherwood number $Sh_m$ in the convergent channels increases as $|\alpha|$ is increased, whereas $Sh_m$ in the divergent channels is almost constant or decreased against $\alpha$. In general, $Sh_m$ shows higher values as the turn clearance is decreased, but the dependence of $Sh_m$ on $C^*$ is rather weak in the divergent channels. The coefficient of pressure loss increases with an increase of $|\alpha|$ in both the convergent and the divergent channels.

2. The distribution of block-averaged Sherwood number $Sh_B$ in the divergent channel is qualitatively similar to that in the parallel-wall channel. The maximum $Sh_B$ appears in Block 9 or 10 located near the turn exit, and it becomes larger with the increase of $\alpha$. In the convergent channel, as $|\alpha|$ is increased, $Sh_B$ increases in the whole test region except for Blocks 9 and 10. The local maximums of $Sh_B$ appear in two locations in and after the turn, and thus the $Sh_B$ distribution is qualitatively different from that in the divergent channel.

3. In the divergent channels, the local Sherwood number *Sh* before the turn (Blocks 1–6) is smaller than that in the parallel-wall channel. In Blocks 9 and 10 near the turn exit, a low-*Sh* region corresponding to a separation bubble, which appears clearly near the divider-wall tip in the parallel-wall channel, becomes smaller in scale, and high-*Sh* regions are formed outside this separation bubble and near the outer wall. *Sh* in these blocks becomes larger as $\alpha$ is increased. After these high-*Sh* regions, *Sh* decreases in the streamwise direction but *Sh* for larger $\alpha$ still keeps higher values.

4. In the convergent channels, *Sh* in the upstream half of the test section is larger than that in the parallel-wall channel. After the turn, a low-*Sh* region corresponding to a rather large separation bubble is formed along the divider wall, while there appears a high-*Sh* region in the opposite outer-wall side. The *Sh* values near the outer wall become larger with the increase of $|\alpha|$. Downstream of this separation bubble, *Sh* shows larger values than that in the corresponding region of the parallel-wall and the divergent channels.

5. In the divergent channels, the global characteristics of *Sh* distributions for different $C^*$ agree qualitatively with one another. The influence of $C^*$ on *Sh* appears only in a limited region near the turn exit, and $\alpha$ is more dominant to the *Sh* distribution than $C^*$. In the convergent channels, the *Sh* distribution is influenced by $C^*$ over the whole region after the turn, and both $\alpha$ and $C^*$ are dominant to the local heat transfer characteristics after the turn.

6. Judging from (i) trade-off between the heat transfer enhancement and pressure loss penalty, and (ii) uniformity in the distribution of local heat transfer rates, the higher heat-transfer performance can be obtained by widening the turn clearance and inclining the divider wall to the convergent side. Under the present experimental condition, the highest heat-transfer performance can be achieved in the convergent channel with $C^* = 1.4$ and $\alpha = -2°$.

## Acknowledgements

The authors wish to thank Mr. N. Shiraki, Research Engineer in the School of Engineering of Nagoya University, for his assistance in producing the experimental apparatus. They also thank Mr. T. Tanaka and Mr. A. Kajita, Chubu Electric Power Inc., for their kind cooperation in conducting this study. This study was supported by the Japanese Ministry of Education through a Grant-in-Aid for Scientific Research (Grant No. 10450083).

## References


[1] D.E. Metzger, C.W. Plevich, C.S. Fan, Pressure loss through sharp 180-deg turns in smooth rectangular channels, J. Eng. Gas Turbines Power 106 (1984) 677–681.

[2] D.E. Metzger, M.K. Sahm, Heat transfer around sharp 180-deg turns in smooth rectangular channels, J. Heat Transfer 108 (1986) 500–506.

[3] C.S. Fan, D.E. Metzger, Effects of channel aspect ratio on heat transfer in rectangular passage with sharp 180-deg turns, ASME Paper, 87-GT-113, 1987.

[4] T.-M. Liou, Y.-Y. Tzeng, C.-C. Chen, Fluid flow in a 180-deg sharp turning duct with different divider thickness, J. Turbomach. 121 (1999) 569–576.

[5] A. Murata, S. Mochizuki, M. Fukunaga, Detailed measurement of local heat transfer in a square-cross-sectioned duct with a sharp 180-deg turn, in: Proceedings of the 10th International Heat Transfer Conference, vol. 4, 1994, pp. 291–296.

[6] T.S. Wang, M.K. Chyu, Heat convection in a 180-deg turning duct with different turn configurations, J. Thermophys. Heat Transfer 8 (1994) 595–601.

[7] T. Astarita, G. Cardone, G.M. Carlomagno, Heat transfer and surface flow visualization around a 180-deg turn in a rectangular channel, in: Heat Transfer in Turbulent Flows, ASME HTD, vol. 318, 1995, pp. 161–168.

[8] S. Mochizuki, A. Murata, R. Shibata, W.-J. Yang, Detailed measurements of local heat transfer coefficients of turbulent flow in smooth and rib-roughened serpentine passages with a 180-deg sharp bend, Trans. Jpn. Soc. Mech. Eng. 64 (1998) 2216–2223 (in Japanese).

[9] T. Astarita, G. Cardone, Thermodynamic analysis of the flow in a sharp 180° turn channel, Exp. Therm. Fluid Sci. 20 (2000) 188–200.

[10] P.R. Chandra, S.C. Lau, J.C. Han, Effect of rib angle on local heat/mass transfer distribution in a two-pass rib-roughened duct, J. Turbomach. 110 (1988) 233–241.

[11] J.C. Han, P.R. Chandra, S.C. Lau, Local heat/mass transfer distributions around sharp 180 deg turns in two-pass smooth and rib-roughened channels, J. Heat Transfer 110 (1988) 91–98.

[12] M.K. Chyu, Regional heat transfer in two-pass and three-pass passages with 180-deg sharp turn, J. Heat Transfer 113 (1991) 63–70.

[13] D.L. Besserman, S. Tanrikut, Comparison of heat transfer measurements with computations for turbulent flow around a 180 deg bend, J. Turbomach. 114 (1992) 865–871.

[14] M. Hirota, H. Fujita, A. Tanaka, S. Araki, T. Tanaka, Local heat (mass) transfer characteristics in rectangular ducts with a sharp 180-degree turn, Energy Convers. Manage. 38 (1997) 1155–1168.

[15] M. Hirota, H. Fujita, A. Syuhada, S. Araki, T. Yoshida, T. Tanaka, Heat/mass transfer characteristics in two-pass smooth channels with a sharp 180-deg turn, Int. J. Heat Mass Transfer 42 (1999) 3757–3770.

[16] M. Hirota, H. Fujita, A. Syuhada, S. Araki, N. Yanagida, T. Tanaka, Heat/mass transfer in serpentine flow passage with a sharp turn (influence of entrance configuration), in: Compact Heat Exchange and Enhancement Technology for Process Industry, 1999, pp. 159–166.

[17] E.M. Sparrow, N. Cur, Turbulent heat transfer in a symmetrically or asymmetrically heated flat rectangular duct with flow separation at inlet, J. Heat Transfer 104 (1982) 82–89.

[18] R.J. Goldstein, H.H. Cho, A review of mass transfer measurements using naphthalene sublimation, Exp. Therm. Fluid Sci. 10 (1995) 416–434.

[19] A. Bejan, Convection Heat Transfer, Wiley, New York, 1984, pp. 326–327.